Ultrafast crystallization of $Ce_{0.9}Zr_{0.1}O_{2-y}$ epitaxial films on flexible technical substrates by pulsed laser irradiation of chemical solution derived precursor layers

Albert Queraltó[1], Angel Pérez del Pino*[,1], Maria de la Mata[1], Jordi Arbiol[1,2], Xavier Obradors[1], and Teresa Puig[1]

[1]Institut de Ciència de Materials de Barcelona, Consejo Superior de Investigaciones Científicas (ICMAB-CSIC), Campus UAB, 08193 Bellaterra, Catalonia, Spain.

[2]Institució Catalana de Recerca i Estudis Avançats (ICREA), Passeig Lluís Companys, 23, 08010

Barcelona, Catalonia, Spain

In this manuscript it is proved that ultraviolet laser irradiation of chemical solution deposited precursor films provides a fast and versatile approach for the fabrication of epitaxial ceria-based thin films on single crystal and flexible YSZ substrates used in coated conductors technologies. The laser-induced epitaxial growth rate of ceria is revealed to be several orders of magnitude larger than in conventional thermal annealing. The main mechanisms responsible for the rapid laser-induced epitaxial nucleation and growth are proposed to be photothermal, though photochemical mechanisms could be also present and would assist the thermal ones. The temperatures and corresponding gradients reached during laser treatments, much higher than in conventional furnace treatments, would provoke enhanced diffusion processes leading to grain boundary recrystallization at much greater growth rates. The described technology could be easily adapted to the industrial sector and it would be cost effective.

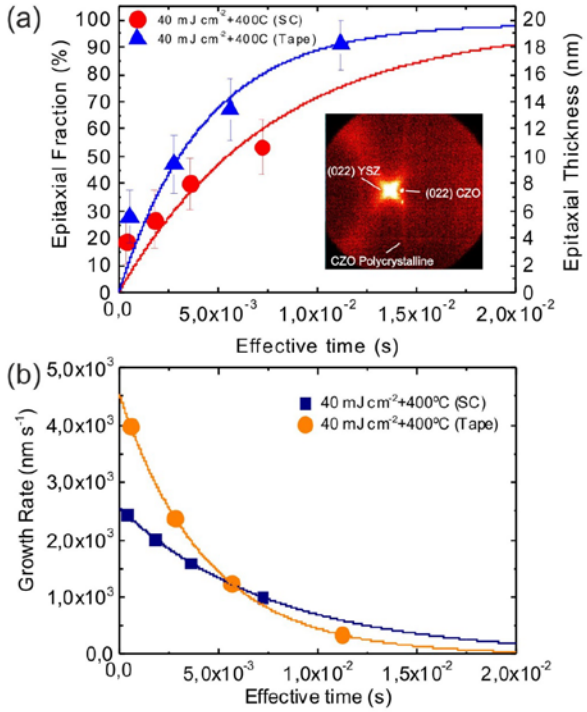

***** Corresponding Author:

Dr. Ángel Pérez del Pino
ICMAB – CSIC, Campus UAB, 08193 Bellaterra, Spain

Tel. +34 935801853; FAX. +34 935805729

E-mail: aperez@icmab.es

http://www.icmab.es/laserprocessing/

Ultrafast crystallization of $Ce_{0.9}Zr_{0.1}O_{2-y}$ epitaxial films on flexible technical substrates by pulsed laser irradiation of chemical solution derived precursor layers

Albert Queraltó[1], Angel Pérez del Pino[*,1], Maria de la Mata[1], Jordi Arbiol[1,2], Xavier Obradors[1], and Teresa Puig[1]*

[1]Institut de Ciència de Materials de Barcelona, Consejo Superior de Investigaciones Científicas (ICMAB-CSIC), Campus UAB, 08193 Bellaterra, Catalonia, Spain.

[2]Institució Catalana de Recerca i Estudis Avançats (ICREA), Passeig Lluís Companys, 23, 08010 Barcelona, Catalonia, Spain

KEYWORDS: laser irradiation, chemical solution deposition, epitaxial crystallization, cerium oxide

ABSTRACT: The epitaxial growth of $Ce_{0.9}Zr_{0.1}O_{2-y}$ (CZO) thin-films on yttria-stabilized zirconia (YSZ) (001) single crystal and YSZ (001)/stainless steel (YSZ/SS) technological substrates is investigated by pulsed laser irradiation of solution-derived cerium-zirconium

precursor layers using a UV Nd:YAG laser source at atmospheric conditions. The influence of laser processing parameters on the morphological and structural properties of the obtained films is studied by atomic force and transmission electron microscopies, as well as X-ray diffractometry. The analyses performed demonstrate that laser treatments enable the epitaxial growth of tens of nm-thick CZO films with a crystallization kinetic process several orders of magnitude faster than that of conventional thermal annealing. Fully epitaxial films are attained using stainless steel (SS) flexible tapes as a substrate. Even though photochemical mechanisms are not fully discarded, it is concluded that photothermal processes are the main contribution responsible for the fast epitaxial crystallization.

INTRODUCTION

Epitaxial growth of CeO_2-based thin films is an important scientific and technological subject as these materials exhibit exceptional functional properties which make them appealing to be used in several applications. For instance, cerium oxide materials display remarkable catalytic activity and high oxygen ionic diffusivity, relevant for sensing and fuel cell devices.[1-4] Additionally, they show high performance optical properties in the IR to UV regions, significant for (electro)optical coatings.[5-9] These oxides are also considered as candidates for replacing silicon dioxide in electronic devices due to their high dielectric constant and compatibility with silicon.[10-12] Finally, Ce-based epitaxial oxide coatings are also employed as buffer layers in complex architectures such as high-temperature superconducting coated conductor tapes, enabling high transport currents with no losses at high magnetic fields.[13] Doping of CeO_2 with

elements like Zr and Gd improves its atomic mobility and avoids the formation of an intermediate carbonate phase which could prevent the growth of highly epitaxial films.[14]

The development of adaptable and cost-efficient methods for the fabrication of epitaxial ceria films is compulsory for some of the previously described applications. Chemical solution deposition (CSD) techniques have attracted a remarkable attention due to their capability for the controlled synthesis of functional epitaxial oxide thin films and multilayers in versatile and low-cost ways. Through these methods it is even possible to grow thin films with complex composition and high crystallinity.[15-17] In essence, CSD consists of: (i) the deposition of a metal organic precursor solution on a substrate with a film thickness determined by the solution concentration; (ii) the precursor pyrolysis at a relatively low temperature; and (iii) the crystallization of oxide films by means of high temperature heat treatments. The main drawbacks of these techniques are that conventional thermal treatments, normally performed using electrical ovens, are time-consuming processes. Moreover, it is not possible to achieve a spatially-resolved decomposition and/or crystallization of materials in a simple way to accomplish the fabrication of miniaturized functional devices straightforwardly.

Laser processing techniques, which are usually characterized by their high accuracy, fast and versatile nature,[18] could overcome the cited limitations of CSD. These approaches present additional advantages such as non-contact processing, localized thermal effect, and low environmental pollution. Laser radiation, when absorbed in a surface material, can lead to very rapid photochemical and/or photothermal mechanisms which can deeply transform its crystalline structure. Accordingly, direct nucleation and growth of functional oxides thin films from laser irradiation of CSD precursors is nowadays a dynamic and increasing research field. Polycrystalline oxide layers of diverse materials including TiO_2, In_2O_3, ITO, $Ba_xSr_{1-x}TiO_3$ or (Pb,

La)(Zr, Ti)O_3 have been mainly produced using CO_2, Nd:YAG and excimer lasers.[19-25] Nevertheless, laser-induced growth of epitaxial thin films is much more complicated, being currently an active exploration area. Recently, UV excimer laser irradiation has been successfully used for the development of epitaxial oxide thin films such as VO_2, Sb-doped SnO_2 and perovskite manganites (LMO, LSMO) working at low substrate temperatures.[26-30] The basic mechanisms involved in epitaxial nucleation and growth of laser annealed functional oxide precursor films are still unclear and they need to be further investigated.

In a previous work, we demonstrated that UV Nd:YAG pulsed laser irradiation can be used for the successful decomposition of CSD-based cerium-zirconium metal-organic precursors films, even down to sub-millimetre surface areas.[31] Further conventional heat treatments led to the fabrication of epitaxial $Ce_{0.9}Zr_{0.1}O_{2-y}$ (CZO) coatings and sub-millimetre structures. In this paper, we report our investigations on laser-induced epitaxial growth of CZO thin films deposited on (001) YSZ single crystal (SC) and (001) YSZ/stainless steel (YSZ/SS) substrates. It is worth noting that the technical YSZ/SS system is typically used in conventional manufacturing to achieve epitaxial CZO film growth, especially for the fabrication of superconducting tapes.[32] The effect of different laser parameters on the morphology and crystallinity of the irradiated material is discussed. Laser processing conditions were optimized in order to achieve epitaxial crystallization of CZO films comparable to that obtained with conventional furnace annealing but with a much shorter effective heating time. The differences between nucleation and crystallization mechanisms in conventional thermal and laser treatments are also discussed. This work evidences that the combination of CSD and laser processing techniques could be a versatile, fast and cost-effective alternative to conventional treatments used in superconducting tape manufacturing and related areas.

EXPERIMENTAL SECTION

Precursor solutions with a total metal concentration of 0.25M were synthesized from cerium (III) and zirconium (IV) acetylacetonate salts (Sigma-Aldrich) diluted in propionic acid and stirred at 50ºC for 30 min. Then, a small amount of solution (14 μL) was spin-coated at 6000 rpm for 2 min on thoroughly cleaned (001)-oriented yttria-stabilized zirconia (YSZ) single crystal (Crystec Gmbh) and YSZ-buffered stainless steel (Bruker Gmbh) 5×5 mm^2 substrates. YSZ buffers were grown on stainless steel by alternating ion beam assisted deposition (ABAD) technique.[33] Single crystal substrates were 0.5 mm-thick, while ABAD-YSZ and stainless steel were about 1 μm and 100 μm in thickness, respectively.

The setup used for laser irradiation consisted of a Nd:YAG laser system (Brilliant, Quantel) which emits pulses with a wavelength of 266 nm, about 3 ns in duration, and at a repetition rate of 10 Hz. The laser beam of 6 mm in diameter had a nearly Gaussian spatial distribution. This means that the laser fluence, i.e. the pulse energy per unit area, decreases with the radial axis, and at the centre of the beam its value (maximum) is two times larger than the average fluence (total pulse energy divided by the beam area). In order to minimize non-uniform crystallization effects due to the Gaussian spatial distribution of the beam, samples were irradiated with a fixed number of accumulated pulses at 1 mm regularly spaced sites to obtain 80% of beam overlapping. Then, the effective number of accumulated pulses per location is about 13 times that of the applied pulses/site due to overlapping. Irradiation of films was performed in air at different substrate temperatures by means of a PID controlled heater (Watlow Ultramic 600). After deposition, the metal-organic Ce-Zr precursor film was laser treated with 10 mJ cm^{-2}

maximum laser fluence, 80% beam overlapping, 100ºC substrate temperature, and 500 pulses/site to fully decompose the organic compounds and obtain a nanocrystalline pyrolyzed film.[31] The range of maximum laser fluences used in this work for further crystallization of the nanocrystalline $Ce_{0.9}Zr_{0.1}O_{2-y}$ films went from 20 to 80 mJ cm^{-2}.

Films morphology was characterized by atomic force microscopy (AFM) using a 5100 equipment from Agilent Technologies set in intermittent contact mode and using silicon tips with a diameter of 10 nm and a force constant of 2.8 N m^{-1}. The analysis of topographic measurements was carried out with the MountainsMap 7.0 software package from Digital Surf. X-ray diffraction (XRD) measurements were performed to evaluate the epitaxial evolution of samples using a Rigaku Rotaflex RU-200BV diffractometer and a GADDS system from Bruker with a 2-dimensional detector, both with a Cu-Kα radiation source (λ = 0.154 nm). In order to study the extent of crystallization of the obtained CZO layers grown by laser processing, we performed high resolution transmission electron microscopy (HRTEM) analyses. On the one hand, samples synthesized on YSZ single crystal substrates were prepared as a cross-section for the TEM observations by mechanical polishing with a final step of ion milling. On the other hand, focused ion beam lamellas were fabricated with layers grown on YSZ/SS tape substrates. In this case, samples were covered by a Pt protecting layer before performing the FIB cut. HRTEM observations were carried out by means of a FEI Tecnai F20 equipment with a field-emission gun operated at 200 kV achieving a lateral resolution of 0.14 nm. Electron energy loss spectroscopy (EELS) analyses were performed in a Jeol J2010F instrument, also working with a field-emission gun and operating at 200 kV in scanning mode (STEM). The system was equipped with a postcolumn Gatan Image Filter (GIF2001) energy spectrometer. Ellipsometry measurements, made with a Sopra GES5E ellipsometer, allowed us to measure the refractive

index (n) and extinction coefficient (κ) of YSZ SC and YSZ/SS substrates. From these parameters, the absorption coefficient ($\alpha = 4\pi\kappa\lambda^{-1}$) and penetration depth (α^{-1}) were also calculated, being λ the radiation wavelength. The optical properties of pyrolyzed nanocrystalline CZO films are already detailed in Ref.[31] Finally, laser-induced thermal processes were simulated using the COMSOL 4.4 Multiphysics software. These calculations involved optical and thermal properties of films and substrates, as well as solving the heat equation by means of finite elements. Thermophysical properties of film and substrates were estimated from Refs.[34-40]

RESULTS AND DISCUSSION

CZO pyrolyzed films deposited on YSZ SC substrates, with a 20 nm effective thickness, exhibit a remarkable surface flatness with typical RMS roughness of about 0.3 nm, as it has been already explained in Ref.[31] The obtained layers are constituted by nanocrystalline CZO material after being pyrolyzed by laser treatments, alike to the films processed by conventional thermal annealing.[35,41] No organic compounds, neither C-impurites, were present in the layer after the pyrolysis process by using these precursors as evidenced by FTIR spectroscopy. Consistently, the pyrolyzed film is mainly composed of Ce-O and Zr-O bonds, in addition to dangling bonds associated to crystalline defects. Cerium oxide is a very stable material, since Ce-O and Zr-O bond dissociation energies are about 795 kJ mol^{-1} (8.3 eV/bond) and 760 kJ mol^{-1} (7.9 eV/bond), respectively,[42] being far larger than the 4.7 eV photon energy corresponding to the employed laser radiation (266 nm). Then, as a first approximation, we can consider the main fundamental interactions between laser light and film-matter being thermally activated (photothermal), though non-thermal (photochemical) processes may also be present predominantly at crystalline defects

where bond dissociation energy would be lower. Photothermal simulations, described in the Supporting Information, were performed by solving the heat equation in CZO/YSZ SC and CZO/YSZ/SS tape systems. As observed in Figure 1, laser pulses provoke similar thermal cycles in both types of film systems (SC and tape), of tens to hundreds of ns in duration. The heating-cooling rates can reach up to 10^{11} ºC s^{-1}, being the cooling time orders of magnitude longer than the heating one due to the difficult heat release through the YSZ thermal insulator material. The maximum temperature developed in the film surface irradiated at room temperature (RT) increases linearly with the laser fluence from about 700ºC at 20 mJ cm^{-2} to around 3000ºC at 80 mJ cm^{-2}, though this last case is probably overestimated due to model constraints. The melting temperature of CZO would be overpassed at laser fluences above 60 mJ cm^{-2}. Moreover, the achieved temperature at the CZO/YSZ interface can be up to 300ºC lower than that of CZO surface at times close to the maximum of the thermal cycle, resulting in temperature gradients up to about 10^{10} ºC m^{-1} across the 20 nm thick CZO film during nanosecond-time intervals. It is worth noting that the radiation penetration depth in pyrolyzed CZO films is about 32 nm, higher than the thickness of the film. This means that about 54% of the incident radiation intensity arrives at the CZO/YSZ interface. Thus, most of this radiation is transmitted and absorbed in the substrate. Consequently, the optical and thermophysical properties of the YSZ substrate play an important role in the system's thermal behavior. As shown in Figure S1, YSZ SC hardly absorbs the incident UV laser radiation, being its penetration depth about 2.5 μm at 266 nm wavelength. Thus, the radiation-induced heating is negligible. However, the YSZ layer grown on SS substrates by ABAD exhibits about three times higher absorption than YSZ SC. This is likely to be caused by the crystalline defects induced in the material during texturation and, hence, the corresponding penetration depth is nearby 800 nm, which is equivalent to the YSZ ABAD film

thickness. As a result, the radiation-induced heating effect will be higher and with a larger contribution to the overall heating of the CZO film. This results in the development of slightly higher temperatures, as well as thermal cycles with a longer duration (Figure 1b).

CZO/YSZ SC systems were irradiated with 80 mJ cm^{-2} laser fluence at RT by accumulation of up to 7000 pulses per site. Figure 2a shows the surface morphology of the irradiated films. The surface reveals the formation of hundreds of nanometers in size planar regions with rounded contours and hundreds of nanometers in size, surrounded by tens of nanometers-sized granular structures with tens of nanometers in size. An increase in the number of accumulated pulses leads to a larger extension of the rounded regions, which gradually acquire polyhedral shape, and a decrease of the RMS roughness from ~6.9 nm at 1000 pulses/site to ~4.7 nm at 7000 pulses/site. In agreement with thermal simulations, laser irradiation at this experimental fluence leads to film temperatures above the CZO melting temperature. Then, the structures with rounded shape would indicate a laser-induced transformation of the CZO material to the molten state, promoting further recrystallization during the cooling process. Similar rounded structures are generally observed in laser melting-resolidification treatments of several types of materials such as metals, semiconductors and polymers.[43-48] The high roughness of the obtained films, as compared to the 0.3 nm initial pyrolyzed layers, could indicate extensive movements of liquid-phase material due to simultaneous action of high temperature gradients, film thermo-mechanical mechanisms, and thermocapillary movements.[18] It must be noted that, according to simulations, the melting temperature of YSZ substrate is not reached in these experimental conditions (Table S1). Figure 2b displays the XRD diffractograms of the samples irradiated with 1000, 3000 and 7000 laser pulses per site. Besides the (002) YSZ (doublet $k_{\alpha 1}$, $k_{\alpha 2}$) located at ~35.0º and weak k_{β} signal at ~31.4º, an intense (002) CZO reflection at 33.4º, as well as the (111) peak of CZO at

28.8º are observed. The intensity of the CZO (002) peak is much higher than that of the (111) orientation, indicating that some epitaxial volume is achieved. As a figure of merit, we show the evolution with the effective heating time of the integrated area of the (002) CZO peak normalized to its value in a sample obtained with conventional furnace treatment at the conditions where low roughness and high quality epitaxial growth is obtained (900ºC during 8 h in oxygen flow).[14,49,50] These values would actually account for the amount of epitaxial CZO material present in the laser processed sample which indeed contributes to the (002) signal. Importantly, the contribution of epitaxial grains to (002) peak signal is highly influenced by their volume and crystallinity. The effective heating time is calculated multiplying the number of accumulated laser pulses by the duration in which the simulated temperature of the irradiated material surpasses 600ºC with the incoming laser pulse. The effect of laser spot overlapping was taken into account for this calculation. For convention, 600ºC has been considered to be the minimum temperature where atomic diffusion is high enough to promote grain growth and the development of high-quality CZO epitaxial crystallization. As observed, the calculated ratio of the laser irradiated layers slowly grows with the effective time, although it is set around 0.1 (10%) in the studied range. These values are low compared to the ones obtained through furnace treatments, but it is also evident that the effective time in laser processing is nearby 7 orders of magnitude lower.

In order to enhance the volume epitaxial fraction and obtain smoother surfaces likely to be compliant with technological applications we have modified the conditions to preferably crystallize CZO films in solid state, i. e. in laser conditions below the melting threshold. For this purpose, laser irradiation of CZO/YSZ SC pyrolyzed layers was performed by accumulation of 1000 pulses/site at 40 mJ cm^{-2} maximum laser fluence at RT, 200ºC and 400ºC substrate

temperature. In all these cases, the calculated maximum temperature of the CZO material is well below its melting threshold (Figure 1b). As observed in Figure S2, the film exhibits granular morphology and decreasing RMS roughness with substrate temperature from ~1.5 nm at RT to ~0.8 nm at 400ºC. XRD analyses show that the increase of substrate temperature certainly leads to a significant augment of the (00l) CZO intensity and corresponding (002) CZO peak normalized area. The rise in the epitaxial quantity (and crystallinity) with substrate temperature would be caused by both the achievement of higher maximum temperatures and the development of longer thermal cycles in the CZO layers. Noteworthy, the XRD diffractogram of a CZO/YSZ pyrolyzed film heated at 400ºC during 1 h shows no CZO reflections pointing to the fact that just heating the substrate to 400ºC does not provoke crystallization. Consequently, in the following experiments we will perform CZO film treatments with 400ºC of substrate temperature.

Laser irradiation of CZO/YSZ SC samples was accomplished at 40 mJ cm^{-2}, 80% beam overlapping, 400ºC of substrate temperature and with a number of 1000, 5000, 10000 and 20000 accumulated pulses per site. Thermal calculations indicate that the laser pulses provoke thermal cycles in the CZO film with maximum temperatures reaching around 1600-1900ºC (Figure 1b). The morphology of the obtained samples is granular (Figure 3a) with grain sizes of about few tens of nm. At the highest number of accumulated pulses, the grains appear to be grouped in domains up to 100-200 nm in size being clearly defined the domain boundaries, similar to furrows. This morphology is rather different to the one obtained by means of furnace treatments, which exhibit a compact terrace-like structure (inset in Figure 3a). The RMS roughness of the laser processed samples is low, about 0.7 nm, and quite constant with the number of accumulated pulses (Figure S3). The granular morphology and low roughness value of these samples would corroborate the advantageous nature of solid state crystal growth processes in these materials for

technological applications, as compared to the morphology obtained in melting-recrystallization processing (Figure 2). XRD characterization shows an intense signal from (002) CZO orientation, with a very weak contribution from the (111) reflection (Figure 3b). As previously observed, the increase of the number of accumulated pulses leads to a rise in the epitaxial (002)-orientation intensity while the (111) peak, perceptible after 1000 pulses/site practically disappears after a higher number of pulses. Accordingly, the (002) CZO normalized area increases with the accumulated number of pulses, i. e. the effective heating time, reaching a ratio nearby 0.35 at 20000 pulses/site (Figure 3c). This indicates that the polycrystalline grains are able to recrystallize to epitaxial ones driven by the minimization of the grain boundary energy, for which the grain size should be kept below a certain size. The obtained '(002) CZO peak normalized area' values are also compared to the ones of samples obtained with 30 min, 4 h and 8 h of conventional heat treatments. The evolution of the (002) CZO normalized area was fitted versus the effective heating time for both laser and furnace treatments, and the temporal derivative of the fitted functions was also calculated and plotted at the corresponding samples' effective heating times (Figure 3d). Roughly, this parameter can be figured out as the growth rate evolution of epitaxial CZO film. As witnessed, laser-treated samples show about thousandfold higher epitaxial growth rates than samples processed by conventional furnace annealing. In both cases, the growth rate decreases with the effective heating time, being this effect more pronounced in laser irradiation processing. The decline of the growth rate can be explained by the reduction of the crystallization driving force (or grain boundary energy) as the film growth proceeds. Furthermore, extrapolating the evolution tendencies, laser treated samples with (002) CZO peak normalized area of 0.6, corresponding to the one obtained with 30 min furnace annealing, would be achieved just after 150 ms of effective laser heating time. These results

indicate that growth of high quality epitaxial CZO not only is possible through laser processing but, moreover, the involved kinetics is much faster than in conventional heating methods.

Since the XRD intensity of (002) CZO peak signal is affected not only by the amount of epitaxial material but also by its crystallinity, an additional method was used to quantify the CZO epitaxial-to-polycrystalline fraction in the laser processed films by means of 2D-XRD epitaxial (spot) and polycrystalline (ring) signals from the same reflection. The calculation details of this method are described in Ref.[51] Figure 4a depicts the evolution of CZO epitaxial fraction in films obtained with 40 mJ cm^{-2} laser fluence, 80% beam overlapping, and 400ºC substrate temperature, as a function of the effective heating time (number of accumulated pulses increasing from 1000 to 20000). As observed, the epitaxial CZO fraction in the films clearly increases with the effective heating time from nearby 20% (~360 μs, 1000 pulses/site) to about 50% (~7.2 ms, 20000 pulses/site). These values are comparable but slightly higher than the corresponding ones obtained in (002) CZO peak normalized area study (Figure 3c). Nevertheless, the samples crystallized by 30 min, 4 h and 8h furnace treatment exhibit a 100% epitaxial fraction, though their normalized area varies from ~0.6 to 1. Therefore, the increase of (002) CZO peak normalized area observed in Figure 3c would actually correspond to epitaxial grain coarsening and elimination of crystalline defects caused by atomic diffusion mechanisms. 2D-XRD studies can be considered to account for the total epitaxial-to-polycrystalline volume in the films and thus it is a better method.

High resolution transmission electron microscopy studies were made to the samples obtained by laser processing with 40 mJ cm^{-2} fluence, 80% beam overlapping, 400ºC substrate temperature and, 1000 pulses/site (Figure 5a-c) and 20000 pulses/site (Figure 5d-f). The sample irradiated with 1000 pulses/site is mainly composed of CZO nanocrystallites with sizes in the 3-8

nm range. The crystallites are randomly oriented as inferred from the observed polycrystalline reflections shown as rings in the power spectra (Fast Fourier Transforms (FFTs)). However, a thin (001)-oriented epitaxial film with irregular surface is actually observed on the film-substrate interface. The thickness of the epitaxial film is about 2-3 nm, corresponding to ~10-15% of the total film thickness. The increase of the number of accumulated laser pulses to 20000 leads to the growth of the epitaxial phase upwards to the film surface, reaching a thickness of about 40-50% of the total film. Noteworthy, the measured thickness values of the epitaxial films closely match with the 'epitaxial fraction' values calculated from XRD methods (Figure 4). The interface roughness between epitaxial and polycrystalline CZO still remains large after 20000 pulses/site, probably due to inhomogeneous temperature gradients and ion diffusion processes during the treatment. Moreover, the power spectra clearly show more intense epitaxial CZO reflections and spotted diffraction rings, indicating the formation of more epitaxial material as well as textured polycrystalline structures.

From all the obtained results is evident that epitaxial growth of CZO nanometric films on YSZ SC substrate is possible by means of pulsed UV laser irradiation, though this system would need, by extrapolation of data from Figure 4a, about 53 ms of effective heating time, what means the accumulation of ~140000 laser pulses/site. Though this effective heating time would be much shorter than the equivalent one through thermal annealing treatments (~2000 s), the use of a high repetition rate laser system would be required for obtaining reasonable processing times. The obtained CZO epitaxial fraction (EF) data (Figure 4a) were fitted by means of Equation 1, previously used to describe a self-limited growth nature in nanocrystalline gadolinia-doped ceria (CGO) films.[52] A_0 = 100 ± 10 % is a prefactor and t_0 parameter is the characteristic crystallization time of the process in which the epitaxially crystallized film reaches 63% of the

total film thickness. Accordingly, a characteristic crystallization time of ~7.7 ms is obtained for the laser-processed samples, whereas values about 420 s, i. e. 5 orders of magnitude longer, are representative for conventional thermal treatments (Figure S4). From these data, we calculated an effective diffusion coefficient (D_{eff}) associated to thermal and laser treatments, as Rupp et al. applied to grain size progression in thermally annealed CGO nanocrystalline films.[52] In this way, effective diffusion coefficients of 2.4×10^{-15} cm^2 s^{-1} and 1.3×10^{-10} cm^2 s^{-1} for conventional and laser treatments are respectively obtained. In concordance to the characteristic crystallization time values, D_{eff} associated to laser treatments is 5 orders of magnitude greater than that of thermal annealing. Besides, Figure 4b presents the temporal derivative of the fitted functions corresponding to the plots shown in Figure 4a, and thus, the overall CZO epitaxial growth rate as a function of effective time. The obtained values, which decrease with effective time, reveal up to 10^3 nm s^{-1} growth rate in laser processed films. These values are about 5 orders of magnitude larger than those obtained by means of conventional heating treatments (Figure S4).

$$EF = A_0\left(1 - e^{-\frac{t}{t_0}}\right) \qquad (1)$$

The origin of such extremely high epitaxial growth rate in laser treatments compared to conventional annealing is still unclear. Some authors claim that photochemical reactions are the main responsible in UV-laser induced growth of epitaxial films.[28,30] They state that the large optical absorption of the substrate is essential for nucleation and growth by laser annealing. However, in our case, the absorption coefficient of the YSZ substrate is rather low and most of the dissociation bond energies present in the material are large compared to the employed photon energy. Hence, we may consider not photochemical but photothermal effects to play a principal role in nucleation and growth kinetics.

High temperature thermal annealing of pyrolyzed CZO films produces the heterogeneous nucleation at the interface with the YSZ substrate and further epitaxial grain growth at the expense of the initial nano-polycrystalline material, leading to a fully epitaxial film after enough heating time.[14,53] Recrystallization and epitaxial growth processes are driven by the free energy difference between epitaxial and polycrystalline material, in addition to the high surface energy of the remaining nanocrystalline layer.[53-56] Since recrystallization from disordered nanocrystallites to epitaxial grains is mainly governed by diffusion across grain boundaries, the temperature of the process is expected to play a major role. As already described, laser irradiation provokes much higher temperatures (~1600-1900ºC) than furnace heating (900ºC) in the treated films which would lead to a significantly greater atomic diffusion process. This behavior is gauged by assuming the dependence of cerium diffusion with temperature in CZO films similar to that reported for Ce in nanocrystalline CGO layers[52] (Figure S5). Figure 6a illustrates the change of Ce diffusion coefficient during the action of the laser pulse in the CZO/YSZ interface and, for comparison, during the action of a conventional thermal annealing treatment (900ºC). The calculations use the simulated evolution of temperature shown in Figure 1b. As revealed, cations would experience a large diffusion increase of 4 orders of magnitude during the action of the laser pulse. Thus, the Ce diffusion coefficient is larger, up to ~2 orders of magnitude, than that in conventional annealing for a time of ~10 ns. As a result, the corresponding diffusion length, which represents the statistical displacement of diffusing atoms and is calculated by means of Equation 2, abruptly increases surpassing that of furnace heating in ~2 ns, reaching then a quasi-steady state (Figure 6b). Conventional annealing would then need about 120 ns to reach the Ce diffusion length of 10^{-4} nm attained with one laser pulse in a time of ~4-5 ns (that is, about 2 orders of magnitude of time difference).

$$L_D = \sqrt{\int_0^\tau D\big(T(t)\big)dt} \qquad (2)$$

The latter results, calculated just considering the variation of the diffusion coefficient with temperature, seem insufficient to entirely explain the 5 orders of magnitude greater D_{eff} and epitaxial growth rates calculated in laser processing as compared to conventional heating. Consequently, further effects may be considered to substantially affect atomic diffusion in laser treatments. It should be stated that diffusing ions experience a drift motion in addition to random diffusion when an external driving force is applied. Besides the gradient of the chemical potential (non-ideal part) between different phases, other driving forces such the ones provoked by an external electric field, stress gradient or temperature gradient may significantly alter the diffusion evolution and, therefore, the growth process.[57] In particular, the driving force developed by the temperature gradient ($F_T \propto \nabla T/T$), essentially negligible in conventional heating, can set the difference with laser annealing. Let us recall that, according to numerical simulations, temperature gradients of 10^{10} ºC m^{-1} can be obtained through film thickness during laser processing. This force would essentially act across the CZO film, moving the ionic species from the surface towards the film-substrate interface where the epitaxial material grows. Though this fact could be a significant contribution to the diffusion - growth difference between laser and furnace techniques, additional mechanisms could be also taken into account to assist the photothermal laser process. Effectively, UV irradiation of crystal boundaries and defects, where optically active dangling bonds can be present, may induce a reactivity enhancement in addition to substantial photo-induced heating at lower laser intensity thresholds than the rest of the crystalline material.[18,58] Moreover, photo-induced electron transitions, which can significantly change the electronic population of the states in the irradiated material, may lower the thermodynamic potential that typically separates two phases.[59] Thus, with long enough lifetime

of the excited electrons, the nucleation energy barrier and its corresponding nucleus critical size can decrease leading to the formation of novel-phase stable nuclei with smaller sizes. As a result, the overall phase transition rate might be increased and this effect would be greater at higher laser fluences. We should remark that these mechanisms, though optically-enhanced, are essentially thermal.

CZO pyrolyzed thin films were also prepared on technological YSZ/SS tapes in the same way as on YSZ SC substrates. In tape system, about 0.8-1 μm thick YSZ is deposited on SS by ABAD process. The crystalline nature of YSZ, shown in Ref.[33], is characterized by a fully polycrystalline structure at the interface with stainless steel sheet (also polycrystalline). YSZ material progressively transforms to (001)-oriented epitaxial configuration upwards to the film surface, where it reveals a completely epitaxial and highly crystalline structure. The pyrolyzed CZO film on tape shows a homogeneous and smooth surface (Figure 7a), with RMS roughness about 0.9 nm, significantly lower than that of initial YSZ/SS, around 1.7 nm. Laser processing of CZO/YSZ/SS samples was performed using the optimized conditions found in CZO/YSZ SC systems, that is, irradiating with 40 mJ cm^{-2} laser fluence, 80% beam overlapping, 400ºC substrate temperature and applying 1000, 5000, 10000 and 20000 accumulated pulses/site. As previously described, thermal assessments point towards similar effects of the laser pulses in the CZO film on tape to the ones triggered in CZO/YSZ SC (Figure 1). However, even though the laser-induced thermal cycles reach just few tens of degrees higher maximum temperatures than in the CZO/YSZ SC system, the effective heating time is revealed to be 40% larger (increase from ~60 ns to ~100 ns, depicted in Figure 1b). This difference in the thermal behavior has been already explained by enhanced radiation absorption (and probably lower thermal conductivity) of YSZ on tape system caused by its intrinsic crystalline defects.

The surface morphology of the CZO films turns to granular when irradiated (Figure 7a), being increased the number of grains and their size with the augment of the accumulated number of laser pulses. Indeed, geometrical boundaries similar to grain grooves firstly appear at low number of accumulated pulses, leading to the further formation of grains as the treatment proceeds. Finally, the surface totally transforms to uniformly distributed grains, of few tens of nm in size, at the highest number, of applied pulses/site (20000). As plotted in Figure S3, the surface RMS roughness progressively increases with the number of accumulated pulses to ~2.3 nm in the studied range of applied pulses. XRD analyses of the obtained samples are presented in Figure 7b. X-ray diffraction patterns show, besides reflections of polycrystalline YSZ and stainless steel substrate, just (002) and (004) peaks of epitaxial CZO material. No additional polycrystalline CZO signal is recorded and the accumulation of laser pulses produces the increase of epitaxial CZO peaks intensity. The (002) CZO peak normalized area calculations reveal slightly higher values than those of CZO/YSZ SC samples obtained with analogous effective heating time. The maximum ratio, obtained by irradiation with 20000 accumulated pulses/site (~11.2 ms effective heating time), is nearby 0.45. On the other hand, the evolution of epitaxial fraction in CZO films grown on tapes, shown in Figure 4a, reveals the achievement of 90-100% at ~11.2 ms effective heating time (20000 pulses/site). Moreover, the CZO epitaxial growth rate on tapes is slightly larger than in YSZ SC (Figure 4b) being, respectively, the characteristic time t_0 about 4.3 and 7.7 ms. The corresponding effective diffusion coefficient is 2.3×10^{-10} cm^2 s^{-1}, ~80% greater than that in YSZ SC. Then, the CZO epitaxial growth can be extended to the full thickness of the film through laser irradiation in similar experimental conditions than using YSZ SC substrates, but with a much lower processing time (required number of pulses multiplied by the laser shooting period). At this stage, secondary processes as

the presence of photoactive defects at the YSZ surface or laser-scattering mechanisms due to the higher roughness of the YSZ/SS surface[18,58] could be considered, which would indeed rise the reached maximum temperatures, as well as the temperature gradients during the developed thermal cycles. The probable decrease of ABAD-YSZ thermal conductivity as compared to YSC SC ones, due to its intrinsic defects and not considered in thermal calculations, might also contribute to this effect. Additional studies should be performed for the verification of these hypotheses.

Finally, HRTEM study of the sample obtained after the accumulation of 20000 pulses per site confirms the growth of a fully epitaxial CZO film with high crystallinity (Figure 8a). Though most of the film is composed of epitaxial (001)-oriented CZO, some minor additional reflections from other orientations are recorded at other locations, as depicted in the power spectra. HRTEM images show a highly crystalline CZO/YSZ heteroepitaxy, though further accumulation of laser pulses would increase the crystallization of the film by elimination of crystalline defects and remaining polycrystals. In Figure 8b, the boundary between two consecutive CZO grains, faceted by {111} lateral surfaces, can be distinguished. This image also reveals the presence of a few nanometers thick CZO continuous layer all over the studied film-substrate interface. Besides, EELS analyses allowed us to obtain the distribution of chemical elements and, congruently, the cerium oxidation state throughout the CZO system. The obtained oxidation state map, depicted in Figure 8c, reveals the presence of Ce^{4+} ions in the entire body of the film. No oxygen vacancies are detected even though the laser processing of the films was performed in air and not in pure oxygen environment, as normally done in conventional annealing methods.

CONCLUSION

The present study demonstrates that the combination of UV laser processing and CSD techniques represents a fast and versatile methodology for the fabrication of epitaxial CZO films on single crystal and technological YSZ flexible substrates. The adaptation of this technology to the industrial environment would be rather easy and cost effective. The laser-induced epitaxial growth rate of CZO is revealed to be up to 10^3 nm s^{-1}, being orders of magnitude larger than in conventional furnace treatment. The main mechanisms responsible for the rapid laser-induced epitaxial nucleation and growth are suggested to be photothermal, though photochemical processes could be also present and would assist the thermal ones. The temperatures and corresponding gradients reached in laser treatments, much higher than in conventional furnace annealing, could also provoke enhanced diffusion processes leading to grain boundary recrystallization at much greater growth rates. Particularly, the epitaxial growth of CZO on YSZ/SS tapes is revealed to be faster than in YSZ SC substrates due to larger temperatures triggered by the laser pulses. The main cause is suggested to be the presence of crystalline defects in the ABAD YSZ buffer layer, which act as radiation absorption centers and add extra thermal energy to the CZO recrystallization process.

ACKNOWLEDGEMENTS

This work was financed by the Ministry of Economy and Competitiveness under the projects MAT2011-28874-C02-01, MAT2014-51778-C2-1-R and Consolider Nanoselect CSD2007-00041, by Generalitat de Catalunya (2009 SGR 770, 2014 SGR 753 and Xarmae) and by the Spanish National Research Council under the Contract No. 200960I015. AQ and MdlM are also

grateful for JAE-Predoc fellowship and European Social Fund program. We acknowledge Bruker Corporation for the supply of the technical substrates through the NMP3-LA-2012-280432 project.

ASSOCIATED CONTENT

Supporting Information.

Description of numerical model used for photothermal simulation, optical parameters of YSZ in SC and YSZ/SS, experimental results on CZO/YSZ SC crystalline structure change after the modification of substrate temperature, RMS roughness of samples irradiated with 40 mJ cm^{-2} laser fluence and 400ºC of substrate temperature, epitaxial fraction of CZO/YSZ SC sample submitted to rapid thermal annealing, temperature evolution of diffusion coefficient of cerium. This information is available free of charge via the Internet at http://pubs.acs.org.

AUTHOR INFORMATION

Corresponding Author

* Tel. +34 935801853

E-mail: aperez@icmab.es

Author Contributions

The manuscript was written through contributions of all authors. All authors have given approval to the final version of the manuscript.

REFERENCES

(1) Chueh, W. C.; Falter, C.; Abbott, M.; Scipio, D.; Furler, P.; Haile, S. M.; Steinfeld. A. High-Flux Solar-Driven Thermochemical Dissociation of CO_2 and H_2O Using Nonstoichiometric Ceria. *Science* **2010**, 330, 1797-1801.

(2) Kang, K. S.; Kim, C. H.; Park, C. S.; Kim. J. W. Hydrogen Reduction and Subsequent Water Splitting of Zr-Added CeO_2. *J. Ind. Eng. Chem.* **2007**, 13, 657-663.

(3) Izu, N.; Shin, W.; Murayama, N. Fast response of resistive-type oxygen gas sensors based on nano-sized ceria powder. *Sens. Actuators B* **2003**, 93, 449-453.

(4) Murray, E. P.; Tsai, T.; Barnett, S. A. A direct-methane fuel cell with a ceria-based anode. *Nature* **1999**, 400, 649-651.

(5) Sainz, M. A.; Duran, A.; Navarro, J. M. F. UV highly absorbent coatings with CeO_2 and TiO_2. *J. Non-Cryst. Solids* **1990**, 121, 315-318.

(6) Al-Robaee, M. S.; Rao, K. N.; Mohan, S. J. Influence of substrate temperature on the properties of oxygen-ion-assisted deposited CeO_2 films. J. *Appl. Phys.* **1992**, 71, 2380.

(7) Zheng, S.; Andersson-Fäldt, A. M.; Stjerna, B.; Granqvist, C. G. Optical properties of sputter-deposited cerium oxyfluoride thin films. *Appl. Opt.* **1993**, 32, 6303-6309.

(8) Krishna, M.; Hartridge, A.; Bhattacharya, A. K. Temperature and ionic size dependence of the properties of ceria based optionic thin films. *Mater. Sci. Eng. B* **1998**, 55, 14-20.

(9) Porqueras, I.; Person, C.; Corbella, C.; Bertran, E. Characteristics of e-beam deposited electrochromic CeO_2 thin films. *Solid State Ion.* **2003**, 165, 131-137.

(10) Cpetti, C. A.; Soltner, H.; Schubert, J.; Zander, W.; Hollricher, O.; Buchal, C.; Schulz, H.; Tellman, N.; Klein, N. High quality epitaxy of $YBa_2Cu_3O_{7-x}$ on silicon-on-sapphire with the multiple buffer layer YSZ/CeO_2. *Appl. Phys. Lett.* **1993**, 63, 1429.

(11) Tye, L.; El-Masry, N. A.; Chikyow, T.; McLarty, P.; Bedair, S. M. Electrical characteristics of epitaxial CeO_2 on Si(111). *Appl. Phys. Lett.* **1994**, 65, 3081.

(12) Skorodumova, N. V.; Ahuja, R.; Simak, S. I.; Abrikosov, I. A.; Johansson, B.; Lundqvist, B. I. Electronic, bonding, and optical properties of CeO_2 and Ce_2O_3 from first principles. *Phys. Rev. B* **2001**, 64, 115108.

(13) Goyal, A.; Paranthaman, M. P.; Schoop, U. The RABiTS Approach: Using Rolling-Assisted Biaxially Textured Substrates for High-Performance YBCO Superconductors. *MRS Bull* **2004**, 29, 552-561.

(14) Coll, M.; Gázquez, J.; Sandiumenge, F.; Puig, T.; Obradors, X.; Espinós, J. P.; Hühne, R. Nanostructural control in solution-derived epitaxial $Ce_{1-x}Gd_xO_{2-y}$ films. *Nanotechnology* **2008**, 19, 395601.

(15) Schwartz, R.; Schneller, T.; Waser, R. Chemical solution deposition of electronic oxide films. *C R Chimie* **2004**, 7, 433-461.

(16) Obradors, X.; Martínez-Julián, F.; Zalamova, K.; Vlad, V. R.; Pomar, A.; Palau, A.; Llordés, A.; Chen, H.; Coll, M.; Ricart, S.; Mestres, N.; Granados, X.; Puig, T.; Rikel, M. Nucleation and mesostrain influence on percolating critical currents of solution derived $YBa_2Cu_3O_7$ superconducting thin films. *Physica C* **2012**, 482, 58-67.

(17) Obradors, X.; Puig, T.; Ricart, S.; Coll, M.; Gazquez, J.; Palau, A.; Granados, X. Growth, nanostructure and vortex pinning in superconducting $YBa_2Cu_3O_7$ thin films based on trifluoroacetate solutions. *Supercond. Sci. Technol.* **2012**, 25, 123001.

(18) Bãuerle, D. *Laser Processing and Chemistry*; Springer: Berlin, 2000.

(19) Ghaith, E. S.; Hayakawa, T.; Kasuga, T.; Nogami, M. Apatite formation on CO_2 laser irradiated titanium oxide films. *Mat. Lett.* **2006**, 60, 194-197.

(20) Ghaith, E. S.; Hayakawa, T.; Kasuga, T.; Nogami, M. Apatite formation on rutile type TiO_2 films formed by laser irradiation. *J. Mater. Sci.* **2006**, 41, 2521-2524.

(21) Tao, X. Y.; Fsaifes, I.; Koncar, V.; Dufour, C.; Lepers, C.; Hay, L.; Capoen, B.; Bouazaoui, M. CO_2 laser-induced crystallization of sol–gel-derived indium tin oxide films. *Appl. Phys. A* **2009**, 96, 741-749.

(22) Baldus, O.; Waser, R. Laser crystallization studies of barium strontium titanate thin films. *J. Eur. Ceram. Soc.* **2004**, 24, 3013-3020.

(23) Imai, H.; Tominaga, A.; Hirashima, H.; Toki, M.; Aizawa, M. Ultraviolet-Laser-Induced Crystallization of Sol-Gel Derived Indium Oxide Films. *J. Sol-Gel Sci. Tech.* **1998**, 13, 991–994.

(24) Bharadwaja, S. S. N.; Dechakupt, T.; Trolier-McKinstry, S. You have full text access to this contentExcimer Laser Crystallized (Pb,La)(Zr,Ti)O_3 Thin Films. *J. Am. Ceram. Soc.* **2008**, 91, 1580-1585.

(25) Kang, M. G.; Cho, K. H.; Oh, S. M.; Do, Y. H.; Kang, C. Y.; Kim, S.; Yoon, S. J. Low-temperature crystallization and electrical properties of BST thin films using excimer laser annealing. *Curr. Appl. Phys.* **2011**, 11, S66-S69.

(26) Nishikawa, M.; Nakajima, T.; Kumagai, T.; Okutani, T.; Tsuchiya, T. Photoassisted chemical solution deposition method for fabricating uniformly epitaxial VO_2 films. *Appl. Phys. A* **2010**, 100, 297–303.

(27) Tsuchiya, T.; Nakajima, T.; Shinoda, K. Electrical properties of Sb-doped epitaxial SnO_2 thin films prepared using excimer-laser-assisted metal–organic deposition. *Appl. Phys. B* **2013**, 113, 333–338.

(28) Nakajima, T.; Tsuchiya, T.; Ichihara, M.; Nagai, H.; Kumagai, T. Epitaxial Growth Mechanism for Perovskite Oxide Thin Films under Pulsed Laser Irradiation in Chemical Solution Deposition Process. *Chem. Mater.* **2008**, 20, 7344–7351.

(29) Tsuchiya, T.; Nakajima, T.; Kumagai, T. Influence of the laser wavelength on the epitaxial growth and electrical properties of $La_{0.8}Sr_{0.2}MnO_3$ films grown by excimer laser-assisted MOD. *Appl. Surf. Sci.* **2009**, 255, 9804–9807.

(30) Nakajima, T.; Shinoda, K.; Tsuchiya T. UV-assisted nucleation and growth of oxide films from chemical solutions. *Chem. Soc. Rev.* **2014**, 43, 2027-2041.

(31) Queraltó, A.; Pérez del Pino, A.; Ricart, S.; Obradors, X.; Puig, T. Laser-induced metal organic decomposition for $Ce_{0.9}Zr_{0.1}O_{2-y}$ epitaxial thin film growth. *J. Alloys Comp.* **2013**, 574, 246–254.

(32) Vlad, V. R.; Zalamova, K.; Coll, M.; Pomar, A.; Palau, A.; Gutierrez, J.; Puig, T.; Obradors, X.; Usoskin, A. Growth of Chemical Solution Deposited $^{TFA}YBCO^{MOD}$ (Ce, Zr)$O_2{}^{ABAD}$ YSZ/SS Coated Conductors. IEEE Transactions on Applied Superconductivity **2009**,19, 3212-3215.

(33) Bartolomé, E.; Vlad, V. R.; Calleja, A.; Aklalouch, M.; Guzmán, R.; Arbiol, J.; Granados, X.; Palau, A.; Obradors, X.; Puig, T.; Usoskin, A. Magnetic and structural characterization of inkjet-printed TFA $YBa_2Cu_3O_{7-x}$/MOD CZO/ABAD YSZ/SS coated conductors. *Supercond. Sci. Technol.* **2013**, 26, 125004.

(34) Acree, W. Jr.; Chickos, J. S. Phase Transition Enthalpy Measurementsof Organic and Organometallic Compounds. Sublimation, Vaporization and Fusion Enthalpies From 1880 to 2010. *J. Phys. Chem. Ref. Data* **2010**, 39, 043101.

(35) Roura, P.; Farjas, J.; Ricart, S.; Aklalouch, M.; Guzman, R.; Arbiol, J.; Puig, T.; Calleja, A.; Peña-Rodríguez, O.; Garriga, M.; Obradors, X. Synthesis of nanocrystalline ceria thin films by low-temperature thermal decomposition of Ce-propionate. *Thin Solid Films* **2012**, 520, 1949-1953.

(36) Manjusha, M. V.; Philip, J. Thermal Properties of Dicalcium Lead Propionate Across the Prominent Transition Temperatures. *Ferroelectric Letters* **2008**, 35, 107-118.

(37) Slade, P. E.; Jenkins, L. T. *Thermal Characterization Techniques;* Marcel Dekker: New York, USA, 1970.

(38) Malaestean, I. L.; Kutluca-Alıcı, M.; Ellern, A.; Van Leusen, J.; Schilder, H.; Speldrich, M.; Baca, S. G.; Kögerler, P. Linear, Zigzag, and Helical Cerium(III) Coordination Polymers. *Cryst. Growth Des.* **2012**, 12, 1593-1602.

(39) Trivedi, S.; Pandey S.Temperature dependent densities of mixtures of 1-butil-3-methylimidazolium hexafluorophosphate + poly(ethylene glycol). *Indian J. Chem*. A **2010,** 49, 731-735.

(40) Assael, M. J.; Gialou, K. Measurement of the Thermal Conductivity of Stainless Steel AISI 304L Up to 550 K. *Int. J. Thermophysics* **2003**, 24, 1145-1153.

(41) Roura, P.; Farjas, J.; Camps, J.; Ricart, S.; Arbiol, J.; Puig, T.; Obradors, X. Decomposition processes and structural transformations of cerium propionate into nanocrystalline ceria at different oxygen partial pressures. *J. Nanopart. Res.* **2011**, 13, 4085-4096.

(42) Dean, J. A. *Lange's handbook of chemistry*, 15th ed., McGraw-Hill: New York, 1999.

(43) György, E.; Pérez del Pino, A.; Serra, P.; Morenza, J. L. Microcolumn development on titanium by multipulse laser irradiation in nitrogen. *J. Mater. Res.* **2003**, 18, 2228-2234.

(44) György, E.; Pérez del Pino, A.; Serra, P.; Morenza, J. L. Structure formation on titanium during oxidation induced by cumulative pulsed Nd:YAG laser irradiation. *Appl. Phys. A* **2004,** 78, 765-770.

(45) György, E.; Mihailescu, I. N.; Serra, P.; Pérez del Pino, A.; Morenza, J. L. Single pulse Nd:YAG laser irradiation of titanium: influence of laser intensity on surface morphology. *Surf. Coat. Tech.* **2002,** 154, 63-67.

(46) Bennett, T. D.; Grigoropoulos, C.P.; Krajnovich, D. J. Near-threshold laser sputtering of gold. *J. Appl. Phys.* **1995**, 77, 849.

(47) Lippert, T. Interaction of Photons with Polymers: From Surface Modification to Ablation. *Plasma Process. Polym.* **2005**, 2, 525-546.

(48) Ryu, S. G.; Gruber, I.; Grigoropoulos, C. P.; Poulikakos, D.; Moon, S. J. Large area crystallization of amorphous Si with overlapping high repetition rate laser pulses. *Thin Solid Films* **2012**, 520, 6724–6729.

(49) Cavallaro, A.; Sandiumenge, F.; Gàzquez, J.; Puig, T.; Obradors, X.; Arbiol, J.; Freyhardt, H. C. Growth Mechanism, Microstructure, and Surface Modification of Nanostructured CeO_2 Films by Chemical Solution Deposition. *Adv. Funct. Mater.* **2006**, 16, 1363-1372.

(50) Coll, M.; Gázquez, J.; Hühne, R.; Holzapfel, B.; Morilla, Y.; García-López, J.; Pomar, A.; Sandiumenge, F.; Puig, T.; Obradors, X. All chemical $YBa_2Cu_3O_7$ superconducting multilayers: Critical role of CeO_2 cap layer flatness. *J. Mater. Res.* **2009**, 24, 1446-1455.

(51) Llordés, A.; Palau, A.; Gázquez, J.; Coll, M.; Vlad, R.; Pomar, A.; Arbiol, J.; Guzmán, R.; Ye, S.; Rouco, V.; Sandiumenge, F.; Ricart, S.; Puig, T.; Varela, M.; Chateigner, D.; Vanacken, J.; Gutiérrez, J.; Moshchalkov, V.; Deutscher, G.; Magen C.; Obradors, X.. Nanoscale strain-induced pair suppression as a vortex-pinning mechanism in high-temperature superconductors. *Nature Mater.* **2012**, 11, 329-336.

(52) Rupp, J. L. M.; Infortuna, A.; Gauckler, L. J. Microstrain and self-limited grain growth in nanocrystalline ceria ceramics. *Acta Mat.* **2006**, 54, 1721-1730.

(53) Gibert, M.; Abellán, P.; Martínez, L.; Román, E.; Crespi, A.; Sandiumenge, F.; Puig, T.; Obradors, X. Orientation and shape selection of self-assembled epitaxial $Ce_{1-x}Gd_xO_{2-y}$ nanostructures grown by chemical solution deposition. *CrystEngComm* **2011**, 13, 6719-6727.

(54) Gibert, M.; Puig, T.; Obradors, X.; Benedetti, A.; Sandiumenge, F.; Huhne, R. Self-Organization of Heteroepitaxial CeO_2 Nanodots Grown from Chemical Solutions. *Adv. Mater.* **2007**, 19, 3937-3942.

(55) Hayun, S.; Ushakov, S. V.; Navrotsky, A. Direct Measurement of Surface Energy of CeO_2 by Differential Scanning Calorimetry. *J Am. Ceram. Soc.* **2011**, 94, 3679-3682.

(56) Obradors, X.; Puig, T.; Gibert, M.; Queraltó, A.; Zabaleta, J.; Mestres, N. Chemical solution route to self-assembled epitaxial oxide nanostructures. *Chem. Soc. Rev.* **2014**, 43, 2200-2225.

(57) Mehrer, H. *Diffusion in Solids*; Springer-Verlag: Berlin Heidelberg, 2007.

(58) Prokhorov, A. M. *Laser heating of metals*; IOP Publishing: Bristol, 1990.

(59) Bennemann, K. H. Photoinduced phase transitions. *J. Phys. Condens. Matter* **2011**, 23, 073202.

FIGURE CAPTIONS

Figure 1. Photothermal simulation of irradiated cerium-zirconia pyrolyzed films. (a) Evolution of the reached maximum temperature as a function of the laser fluence in films deposited on YSZ SC and YSZ/SS tape. Inset: spatial distribution of temperatures in the CZO/YSZ SC system irradiated with 40 mJ cm^{-2} @ 6 ns. (b) Temporal evolution of the temperature of films deposited on SC and tape architectures, when irradiated with 40 mJ cm^{-2} at 400ºC substrate temperature.

Figure 2. Pyrolyzed CZO films deposited on YSZ SC, irradiated with 80 mJ cm^{-2} at room temperature. (a) AFM images of samples obtained with different number of pulses per site, and (b) their respective XRD diffractograms and analysis of the normalized area of (002) CZO peak compared to the one of sample obtained by conventional furnace annealing (900ºC, oxygen atmosphere, and 8 h treatments).

Figure 3. CZO obtained by irradiation of pyrolyzed films on YSZ SC with 40 mJ cm^{-2} laser fluence, and heated to 400ºC during processing. (a) AFM images of the samples obtained with different number of accumulated pulses per zone. Inset: image of a typical sample crystallized by conventional furnace annealing (900ºC, 8 h). (b) XRD diffractograms of the samples irradiated with different number of accumulated pulses, as well as a pyrolyzed film heated at 400ºC during 1 h. (c) (002) CZO peak normalized areas of the laser and furnace (30 min, 4 h and 8 h) obtained films and (d) their corresponding temporal derivative.

Figure 4. (a) Epitaxial fraction of samples obtained by laser treatment. Inset: Typical 2D-XRD image centered at (022) Bragg reflections of CZO for the quantification of the randomly oriented crystals' fraction. (b) Temporal derivative evolution of epitaxial fraction as a function of effective heating time.

Figure 5. HRTEM images and power spectra of samples obtained by irradiation of CZO pyrolyzed films deposited on YSZ SC with 40 mJ cm^{-2} laser fluence, 400ºC substrate temperature and (a, b, c) 1000, and (d, e, f) 20000 accumulated pulses per zone. (b) and (e) are filtered images (IFFTs) to highlight the presence of the CZO epitaxial fraction.

Figure 6. (a) Diffusion coefficient and (b) diffusion length evolution with time for laser (40 mJ cm^{-2} laser fluence, 400ºC substrate temperature, in SC and Tape configurations) and furnace (900ºC) treatments.

Figure 7. Samples obtained by laser irradiation of CZO films deposited on YSZ/SS tape with 40 mJ cm^{-2} laser fluence and 400ºC substrate temperature, in addition to just pyrolyzed film. (a) AFM images, and (b) XRD diffractograms in addition to related (002) CZO peak normalized area plot (including the values of films grown on YSZ SC in the same experimental conditions for comparison).

Figure 8. HRTEM images and corresponding power spectra of the sample grown on tape by irradiating with 40 mJ cm^{-2}, at 400ºC substrate's temperature, and accumulating 20000 pulses per zone. Areas with different degree of crystallization are shown in (a), and a more general view of the morphology of the layer can be seen in (b) and (c). The inset in (c) shows a cerium oxidation state map obtained by EELS.

FIGURES

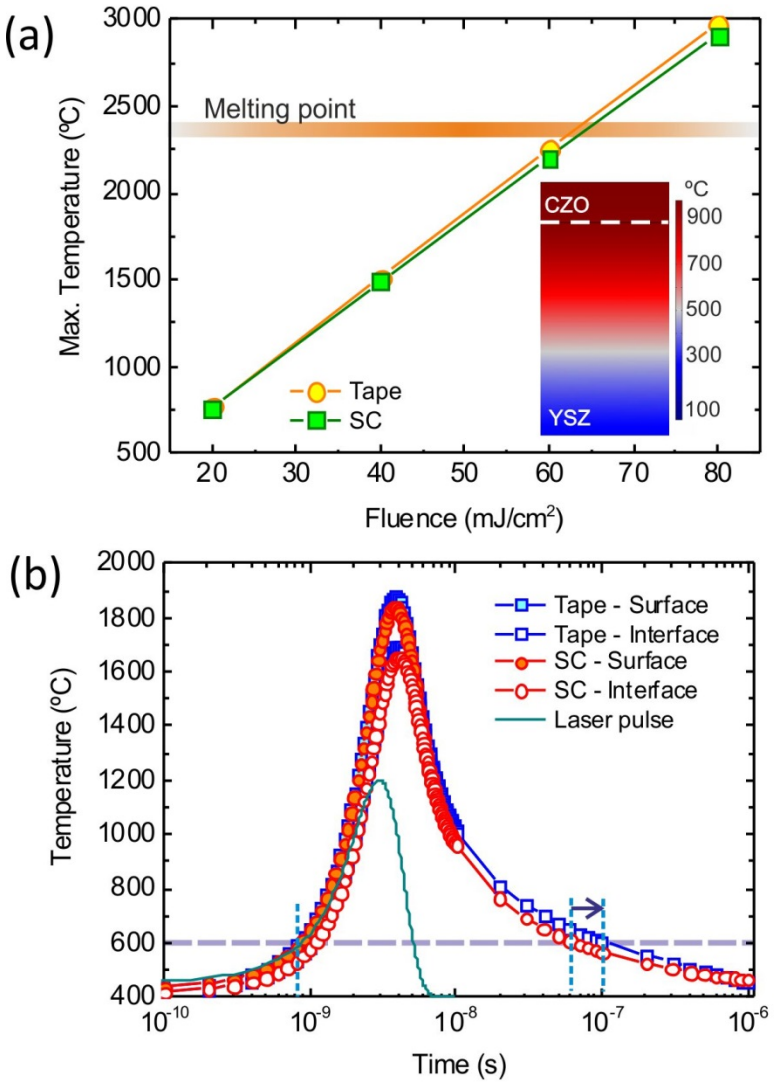

Figure 1.

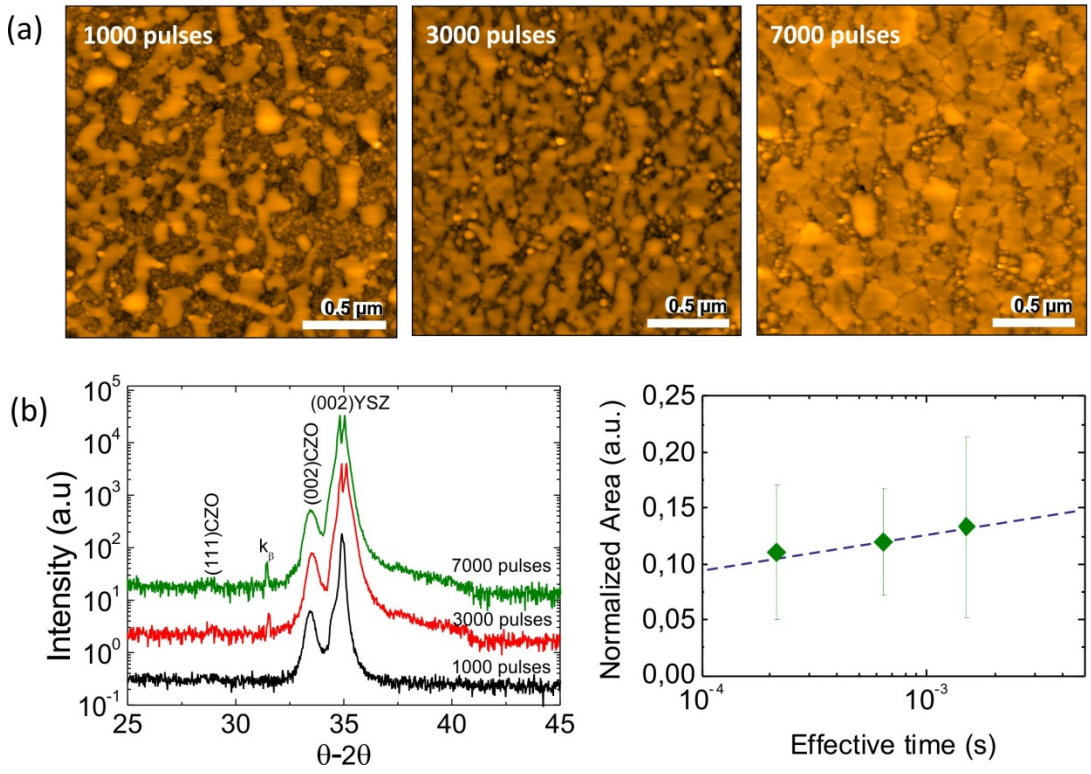
(a)
1000 pulses
0.5 µm
3000 pulses
0.5 µm
7000 pulses
0.5 µm
(b)
Intensity (a.u)
θ-2θ
(111)CZO
k_β
(002)CZO
(002)YSZ
7000 pulses
3000 pulses
1000 pulses
Normalized Area (a.u.)
Effective time (s)

Figure 2.

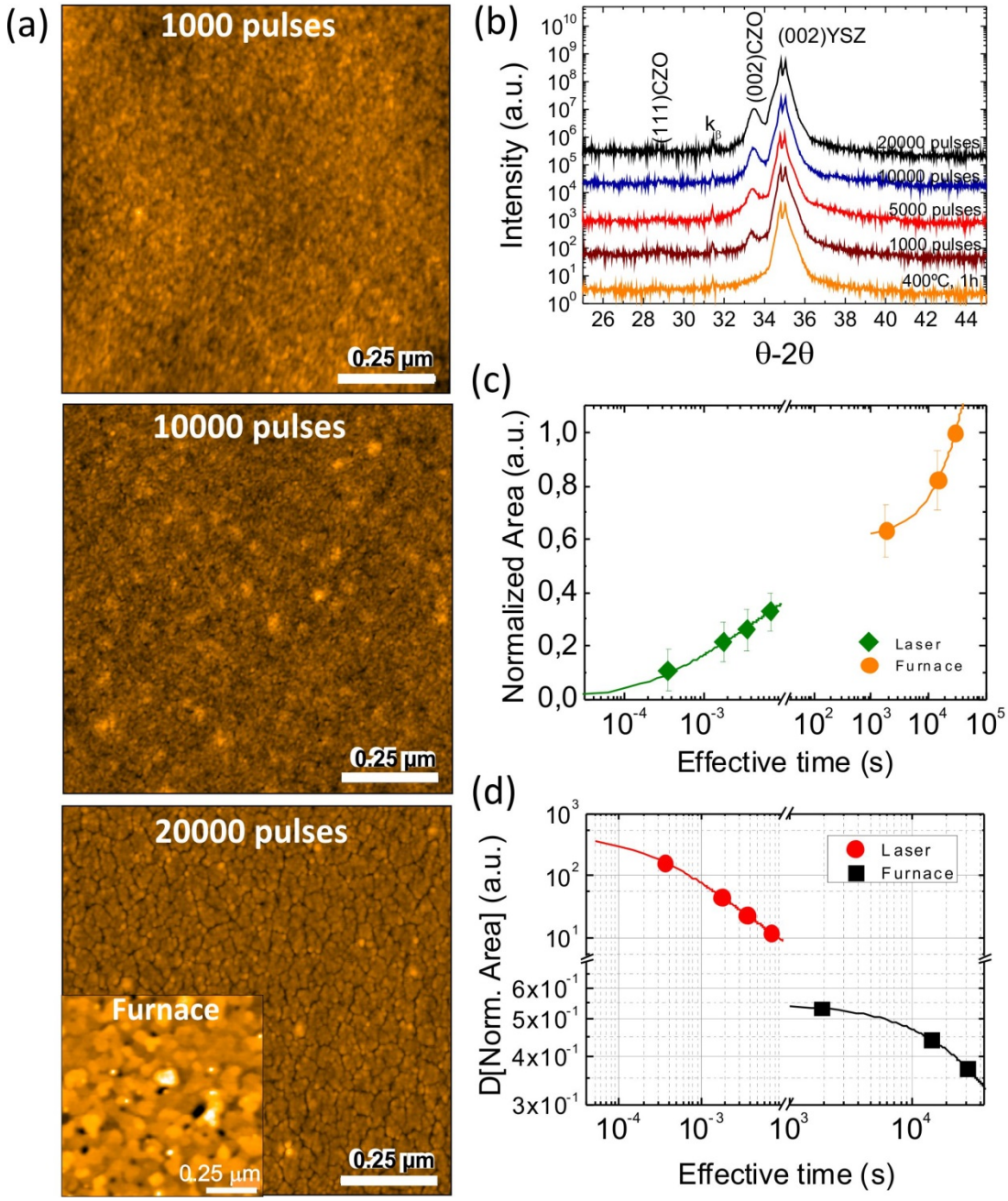
(a)
1000 pulses
0.25 µm
10000 pulses
0.25 µm
20000 pulses
Furnace
0.25 µm
0.25 µm
(b)
Intensity (a.u.)
(111)CZO
k_β
(002)CZO
(002)YSZ
20000 pulses
10000 pulses
5000 pulses
1000 pulses
400°C, 1h
θ-2θ
(c)
Normalized Area (a.u.)
Laser
Furnace
Effective time (s)
(d)
D[Norm. Area] (a.u.)
Laser
Furnace
Effective time (s)

Figure 3.

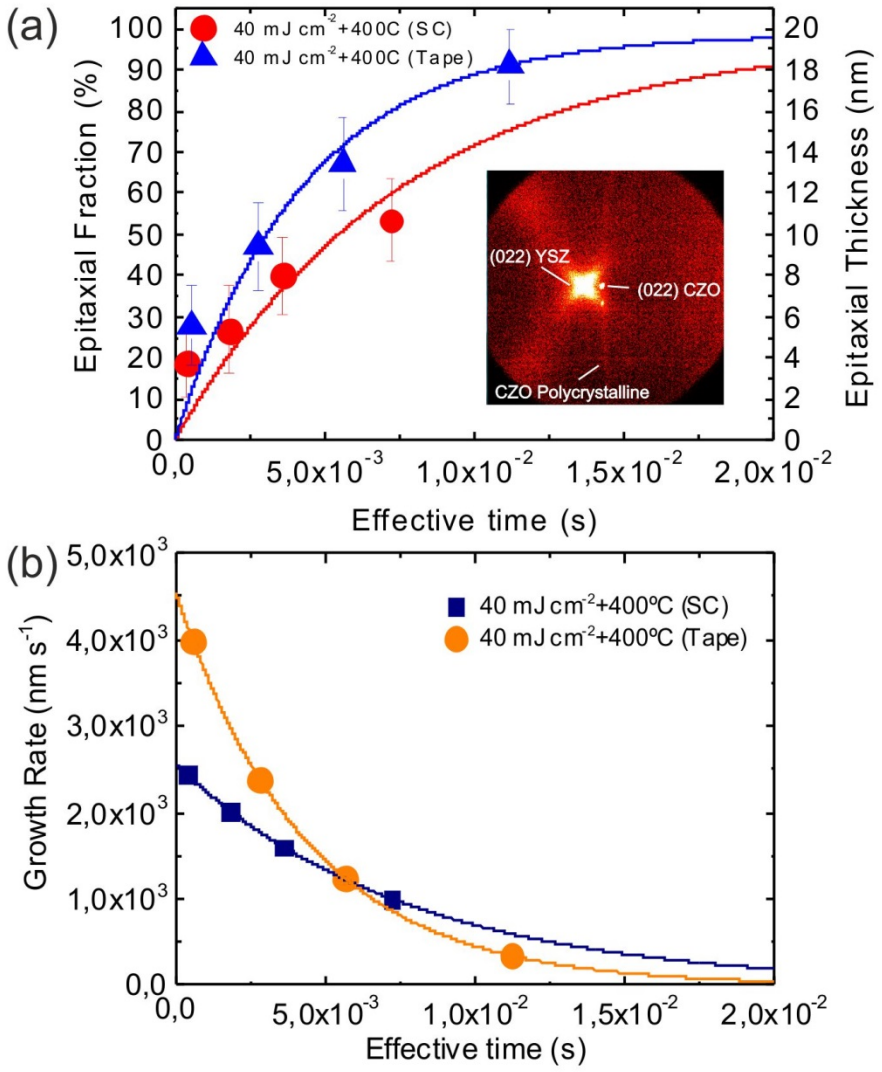
(a)
40 mJ cm-2+400C (SC)
40 mJ cm-2+400C (Tape)
Epitaxial Fraction (%)
Epitaxial Thickness (nm)
(022) YSZ
(022) CZO
CZO Polycrystalline
Effective time (s)
(b)
40 mJ cm-2+400ºC (SC)
40 mJ cm-2+400ºC (Tape)
Growth Rate (nm s-1)
Effective time (s)

Figure 4.

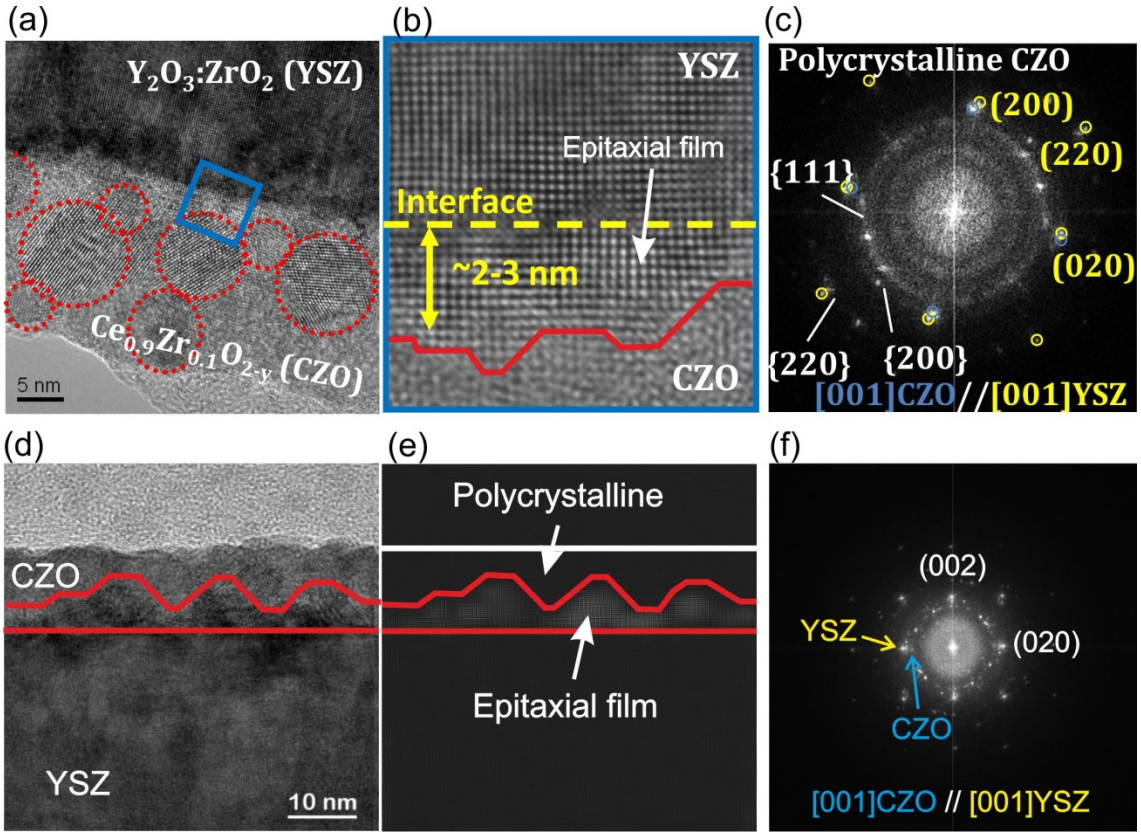
(a)
Y_2O_3:ZrO_2 (YSZ)
$Ce_{0.9}Zr_{0.1}O_{2-y}$ (CZO)
5 nm
(b)
YSZ
Epitaxial film
Interface
~2-3 nm
CZO
(c)
Polycrystalline CZO
(200)
(220)
{111}
(020)
{220}
{200}
[001]CZO//[001]YSZ
(d)
CZO
YSZ
10 nm
(e)
Polycrystalline
Epitaxial film
(f)
(002)
YSZ
(020)
CZO
[001]CZO // [001]YSZ

Figure 5.

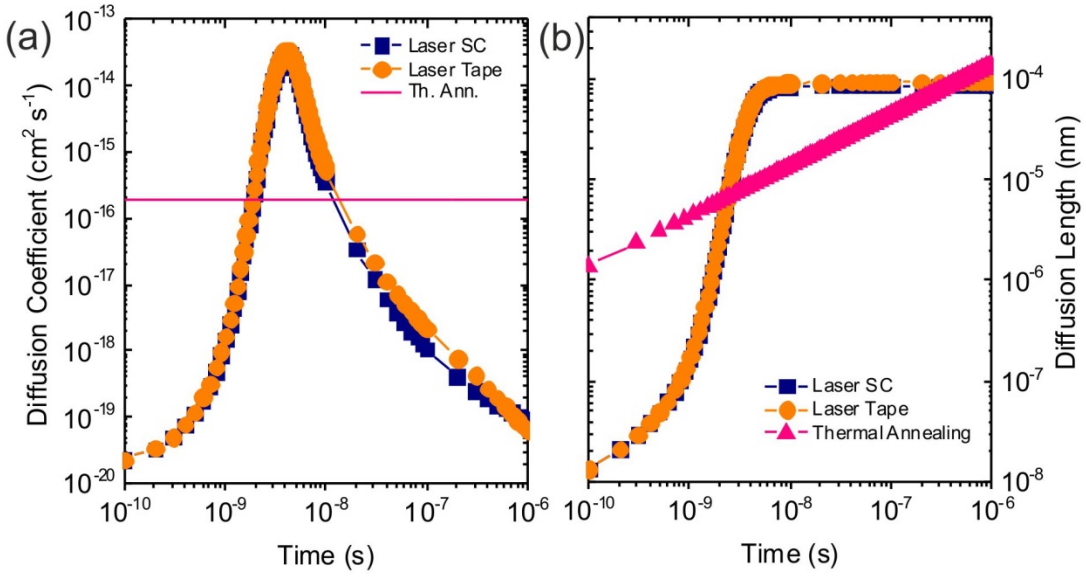
(a)
Laser SC
Laser Tape
Th. Ann.
Diffusion Coefficient (cm^2 s^{-1})
Time (s)
(b)
Laser SC
Laser Tape
Thermal Annealing
Diffusion Length (nm)
Time (s)

Figure 6.

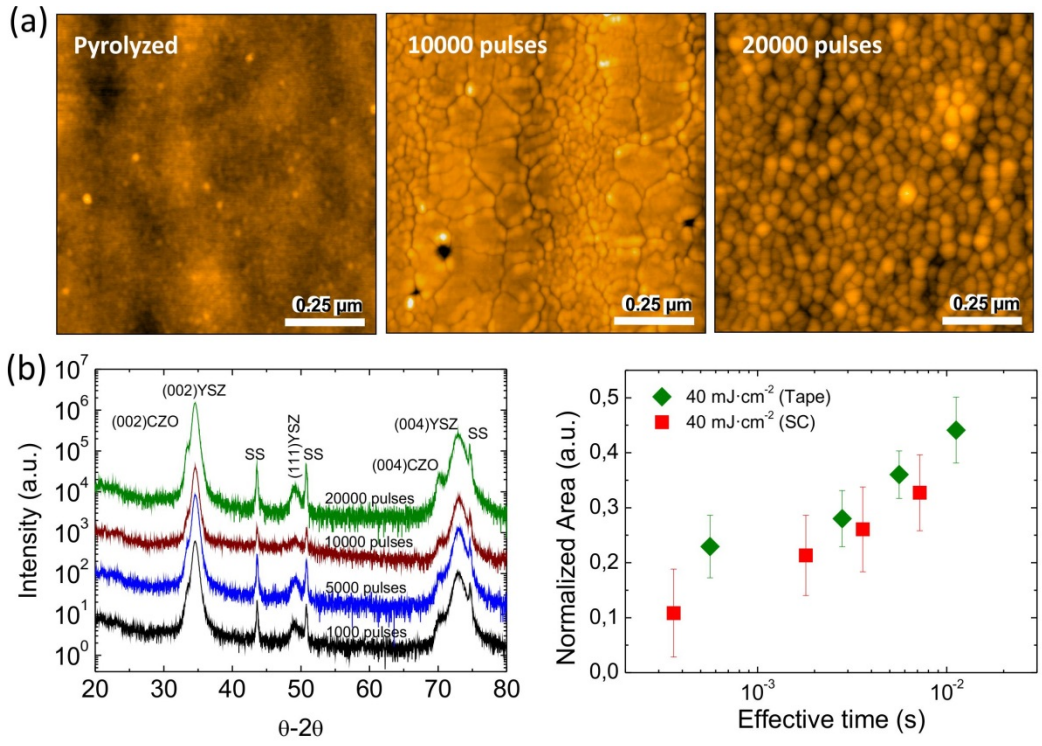
(a)
Pyrolyzed
0.25 µm
10000 pulses
0.25 µm
20000 pulses
0.25 µm
(b)
Intensity (a.u.)
(002)YSZ
(002)CZO
SS
(111)YSZ
SS
(004)YSZ
SS
(004)CZO
20000 pulses
10000 pulses
5000 pulses
1000 pulses
θ-2θ
Normalized Area (a.u.)
40 mJ·cm-2 (Tape)
40 mJ·cm-2 (SC)
Effective time (s)

Figure 7.

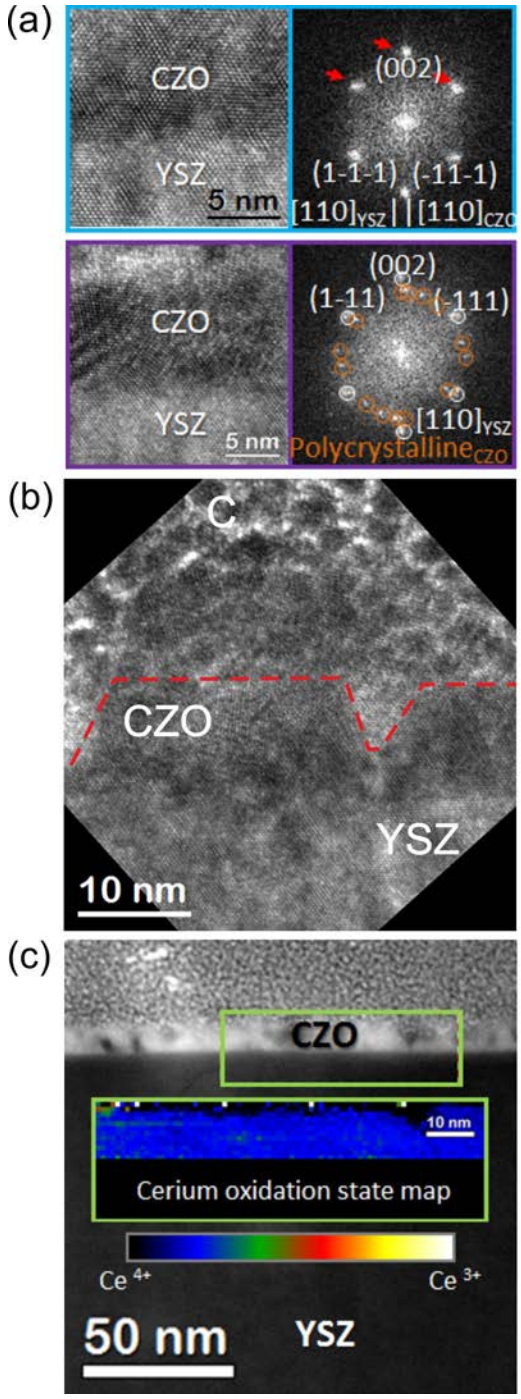
(a)
CZO
YSZ
5 nm
(002)
(1-1-1)
(-11-1)
[110]YSZ||[110]CZO
CZO
YSZ
5 nm
(002)
(1-11)
(-111)
[110]YSZ
PolycrystallineCZO
(b)
C
CZO
YSZ
10 nm
(c)
CZO
10 nm
Cerium oxidation state map
Ce 4+
Ce 3+
50 nm
YSZ

Figure 8.

For Table of Contents Use Only

Ultrafast crystallization of $Ce_{0.9}Zr_{0.1}O_{2-y}$ epitaxial films on flexible technical substrates by pulsed laser irradiation of chemical solution derived precursor layers

Albert Queraltó[1], Angel Pérez del Pino*[,1], Maria de la Mata[1], Jordi Arbiol[1,2], Xavier Obradors[1], and Teresa Puig[1]

[1]Institut de Ciència de Materials de Barcelona, Consejo Superior de Investigaciones Científicas (ICMAB-CSIC), Campus UAB, 08193 Bellaterra, Catalonia, Spain.

[2]Institució Catalana de Recerca i Estudis Avançats (ICREA), Passeig Lluís Companys, 23, 08010 Barcelona, Catalonia, Spain

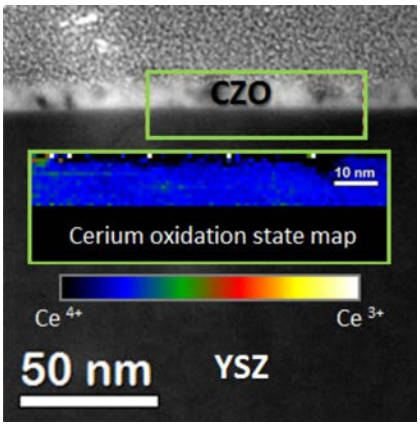

Synopsis

A fast and versatile method for obtaining Zr-doped ceria epitaxial thin films on YSZ single crystal and bendable YSZ / stainless steel technological substrates is proposed through the laser irradiation of solution derived precursor coatings. The specific laser-induced mechanisms taking place in the irradiated material lead to crystallization rates several orders of magnitude faster than that of conventional thermal treatments.